Electronic Supplementary Information

Multifunctional Lanthanide MOF luminescent sensor built by structural design and energy level regulation of ligand

Xueguang Liu[a†], Wei Liu[b†], Yao Kou[1], Xiaoshan Yang[a], Zhenghua Ju[a],*

Weisheng Liu[a]*

[a]Key Laboratory of Nonferrous Metal Chemistry and Resources Utilization of Gansu Province and State Key Laboratory of Applied Organic Chemistry, Key Laboratory of Special unction Materials and Structure Design, Ministry of Education, College of Chemistry and Chemical Engineering, Lanzhou University, Lanzhou 730000, China. Lanzhou 730000 (P.R. China). *E-mail: liuws@lzu.edu.cn.

[b]Institute of National Nuclear Industry, Frontiers Science Center for Rare Isotope, School of Nuclear Science and Technology, Key Laboratory of Special Function Materials and Structure Design, Ministry of Education, Lanzhou University, 730000, Lanzhou, China.

[†]These authors contributed equally to this work.

* Corresponding authors:
E-mail for Weisheng Liu: liuws@lzu.edu.cn
* Corresponding authors:
E-mail for Wei Liu: l_w@lzu.edu.cn

Materials and Instrumentation: All solvents and reagents were commercially available A.R. grade and used without further purification unless otherwise noted. Preparation of stock solutions: All the analytic nitro explosives solutions were prepared by separately dissolving each of them in DMAC with a concentration of 0.1 M and 0.01M. Luminescence spectra were measured using a Hitachi F-7000 luminescence spectrometer. Fluorescent quantum yield was determined by an absolute method using an integrating sphere on FLS920 of Edinburgh Instrument. UV-visible spectra were recorded using an Agilent Cary 5000 spectrophotometer. The FT-IR spectra were recorded from KBr pellets in the range from 4000 to 500 cm^{-1} on a Bruker VERTEX 70 spectrometer. Powder X-Ray diffraction (PXRD) patterns were collected with a PAN alytical X'Pert Pro Diffractometer operated at 40 kV and 40 mA with Cu Kα radiation. Thermogravimetric analyses (TGA) were obtained on a NETZSCH STA 449 F3 Jupiter® under a N_2 atmosphere.

X-ray Structural Crystallography: The single-crystal X-ray diffraction data was collected on a XtaLAB Synergy R, DW system, HyPix diffractometer. The crystal was kept at 149.99(10) K during data collection. Using Olex2 [1], the structure was solved with the SHELXT [2] structure solution program using Intrinsic Phasing and refined with the SHELXL [3] refinement package using Least Squares minimisation.
1. Dolomanov, O.V., Bourhis, L.J., Gildea, R.J, Howard, J.A.K. & Puschmann, H. (2009), J. Appl. Cryst. 42, 339-341.
2. Sheldrick, G.M. (2015). Acta Cryst. A71, 3-8.
3. Sheldrick, G.M. (2015). Acta Cryst. C71, 3-8.

Calculations of Luminescent Quantum Yield: Luminescent quantum yield data was measured in the solid state at 298K, and the emission was monitored from 450 to 650 nm. The overall luminescent quantum yields of the solid-state samples were determined by an absolute method using an integrating sphere on FLS920 of Edinburgh Instrument (150 mm diameter, $BaSO_4$ coating) and acquired using the following equation:

$\Phi_{overall} = (A_H) / (R_{ST} - R_H)$ (S1)

where A_H is the area under emission spectrum of the sample and R_{ST} and R_H are diffuse reflectance of the reflecting standard and the sample, respectively[1-2].

Additional Figures and Schemes:
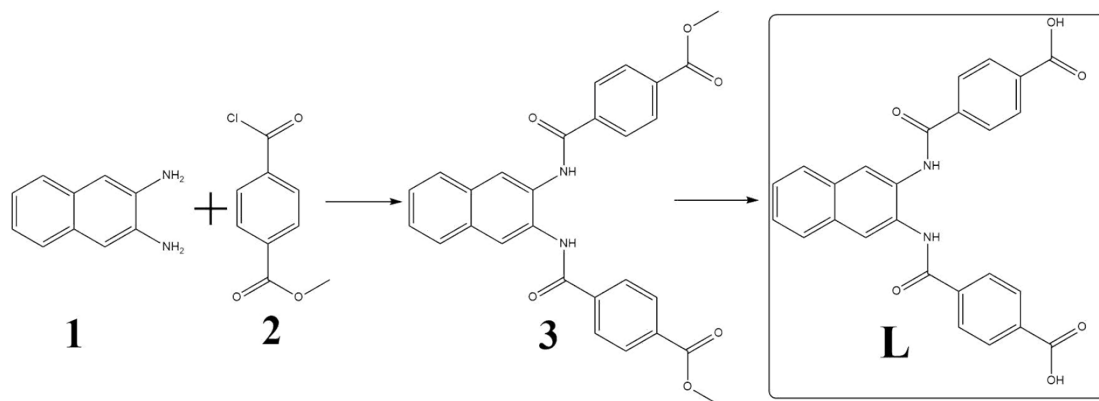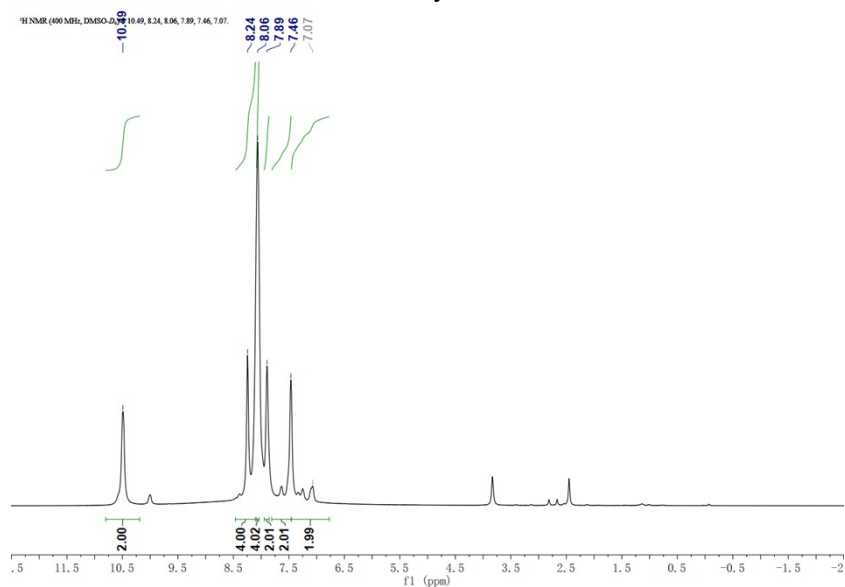

Scheme S1. Synthesis of L

Fig S1. ^{1}H NMR spectra of L^{2-} recorded in DMSO.
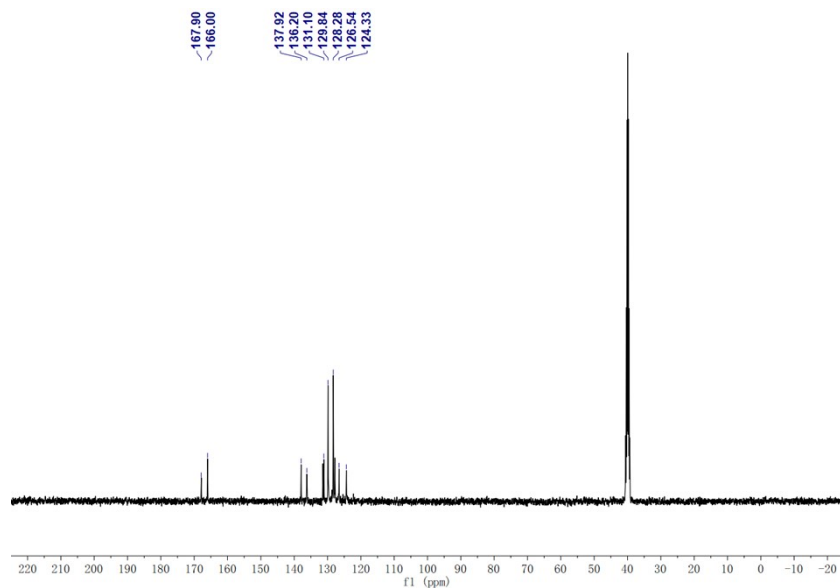
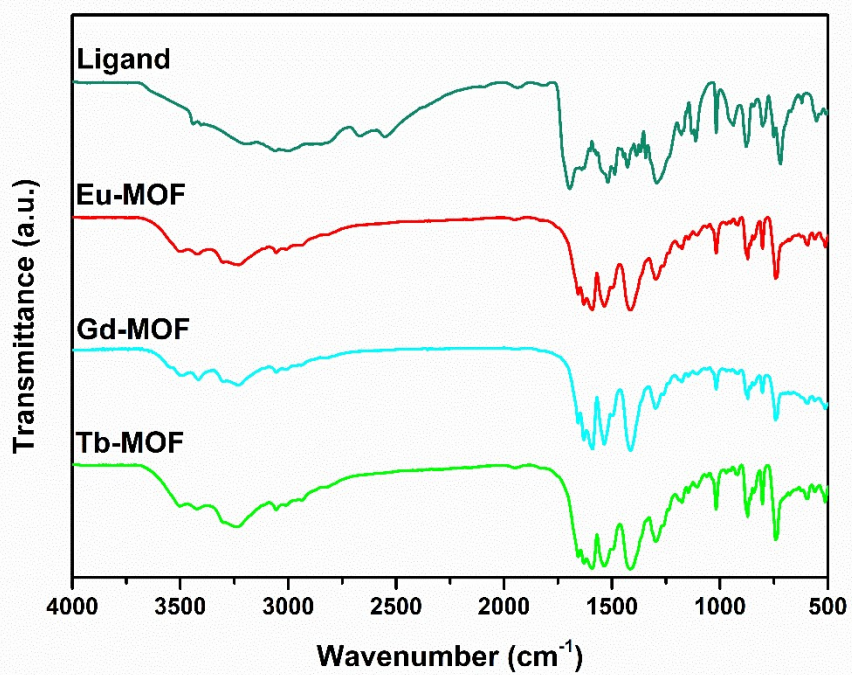**Fig S2.** ^{13}C NMR spectra of L^{2-} recorded in DMSO.

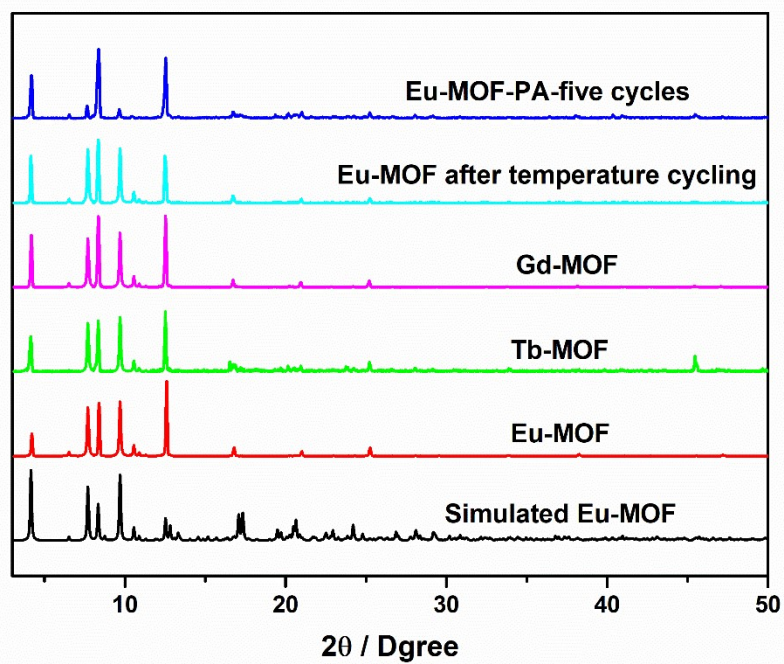**Fig S3.** IR spectra of the Ln-MOFs and the ligand.

Fig S4. The PXRD patterns of the Ln-MOF (Ln = Eu, Tb, Gd) and the Eu-MOF after five cycles experiment for detecting PA and temperature sensing.
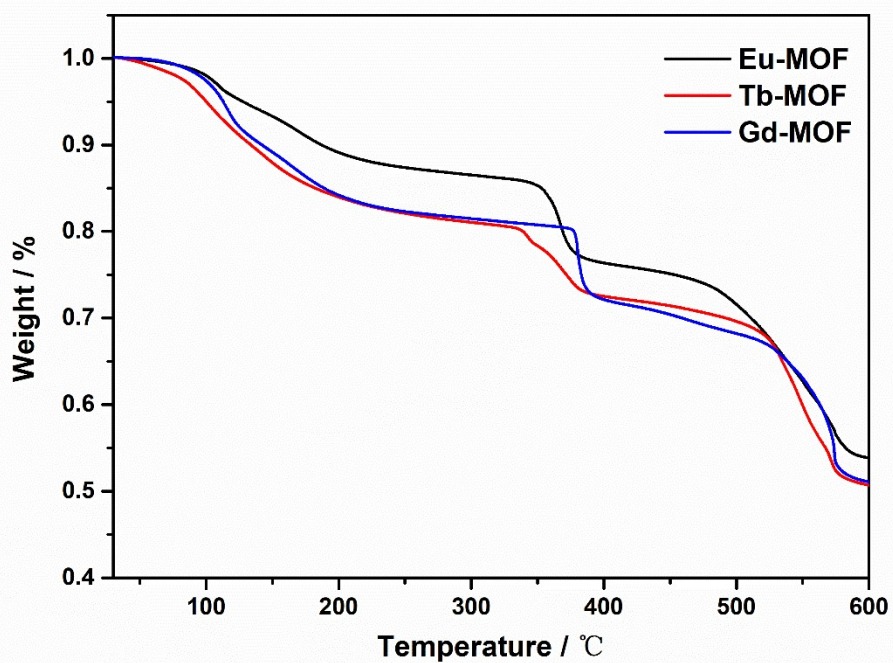

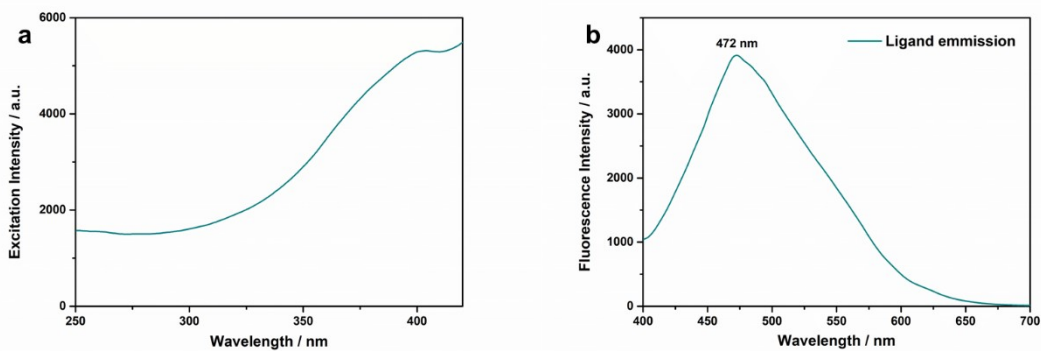**Fig S5.** TGA plot of the Ln-MOF (Ln = Eu, Tb, Gd)

Fig S6. (a) The solid-state excitation spectrum of the ligand at room temperature (λ_{em} = 472 nm).
(b) The solid-state emission spectrum of the ligand at room temperature (λ_{ex} = 365 nm).
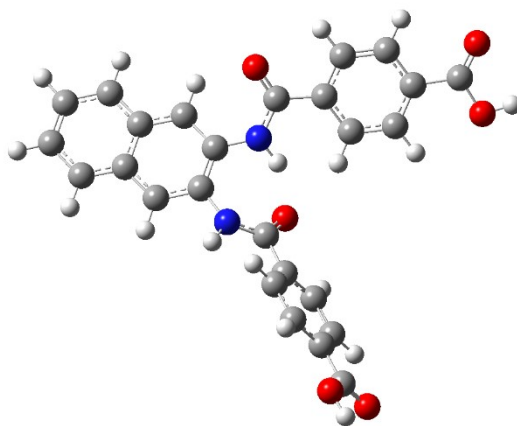

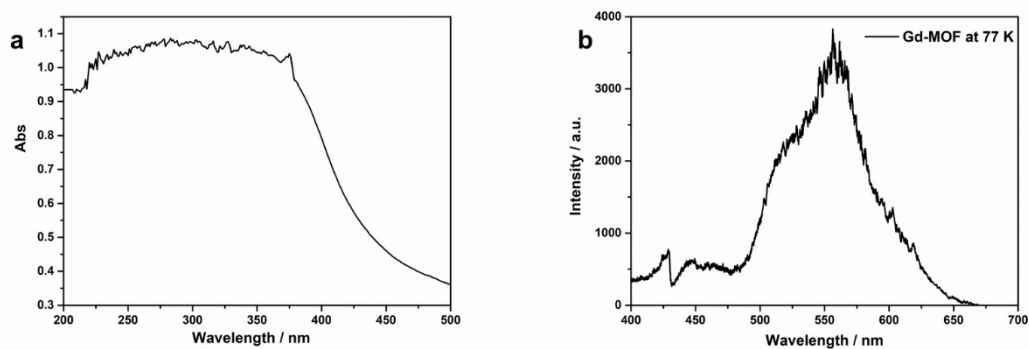**Fig S7**. The optimized geometry of the free ligand

Fig S8. (a) UV-Vis absorption spectrum of the ligand. (b) phosphorescence spectrum of the Gd-MOF at 77K.

Fig S9. (a) The solid-state excitation spectrum of the Eu-MOF at room temperature (λ_{em} = 614 nm). (b) The solid-state emission spectrum of the Eu-MOF at room temperature (λ_{ex} = 365 nm).
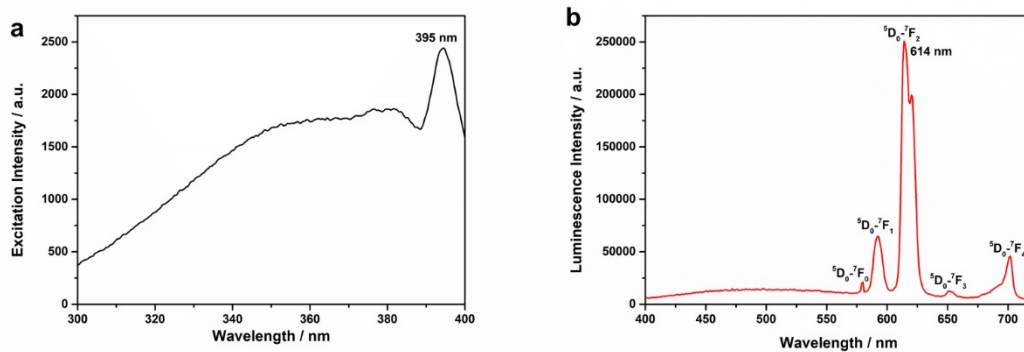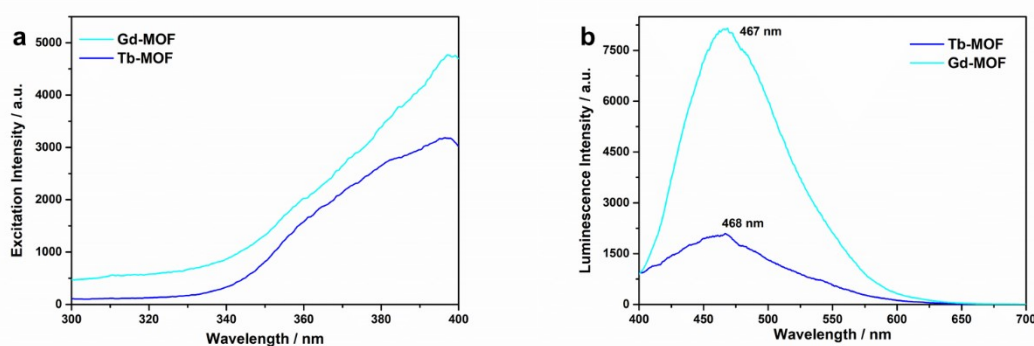

Fig S10. (a) The solid-state excitation spectrums of the Tb-MOF and Gd-MOF at room temperature (λ_{em} = 468 nm). (b) The solid-state emission spectrums of the Tb-MOF and Gd-MOF at room temperature (λ_{ex} = 365 nm).
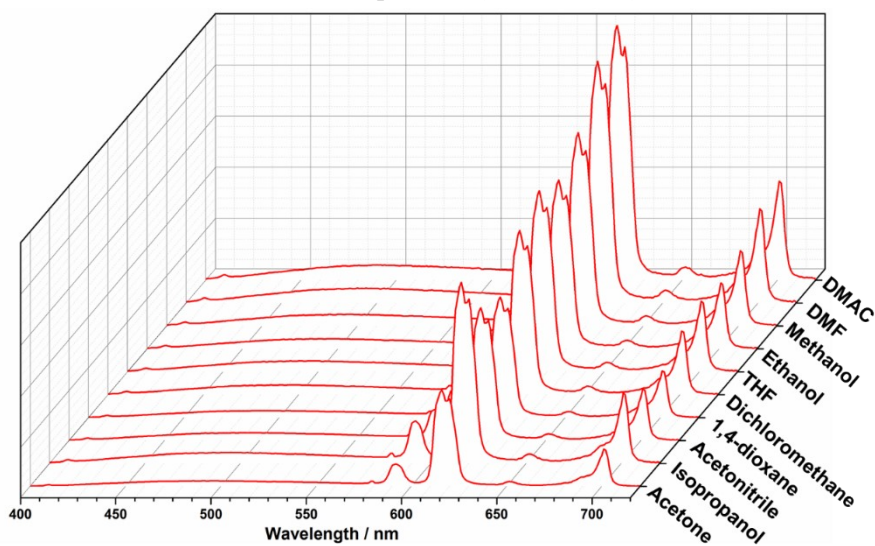
Fig S11. The luminescence spectra of the Eu-MOF in different organic solvents.

Fig S12. (a) The luminescence spectra of the Eu-MOF recorded with different concentrations of p-nitrophenol (0-0.5 mM) in DMAC. (b) SV plot of I_0/I vs increasing concentrations of p-nitrophenol.
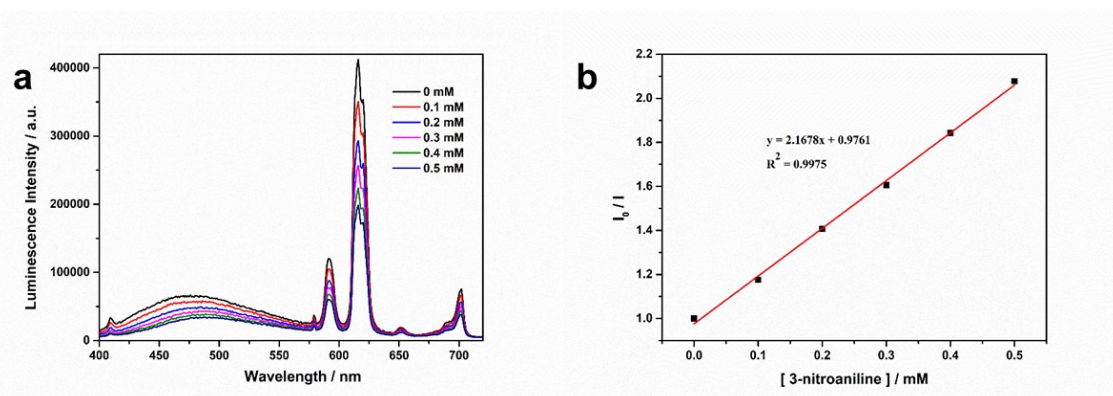
Fig S13. (a) The luminescence spectra of the Eu-MOF recorded with different concentrations of 3-nitroaniline (0-0.5 mM) in DMAC. (b) SV plot of I_0/I vs increasing concentrations of 3-nitroaniline.
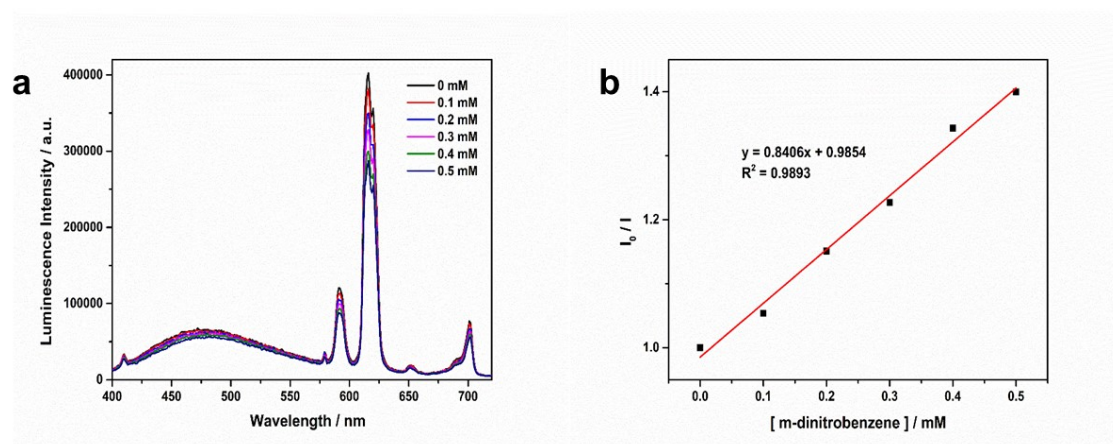
Fig S14. (a) The luminescence spectra of the Eu-MOF recorded with different concentrations of m-dinitrobenzene (0-0.5 mM) in DMAC. (b) SV plot of I_0/I vs increasing concentrations of m-dinitrobenzene.
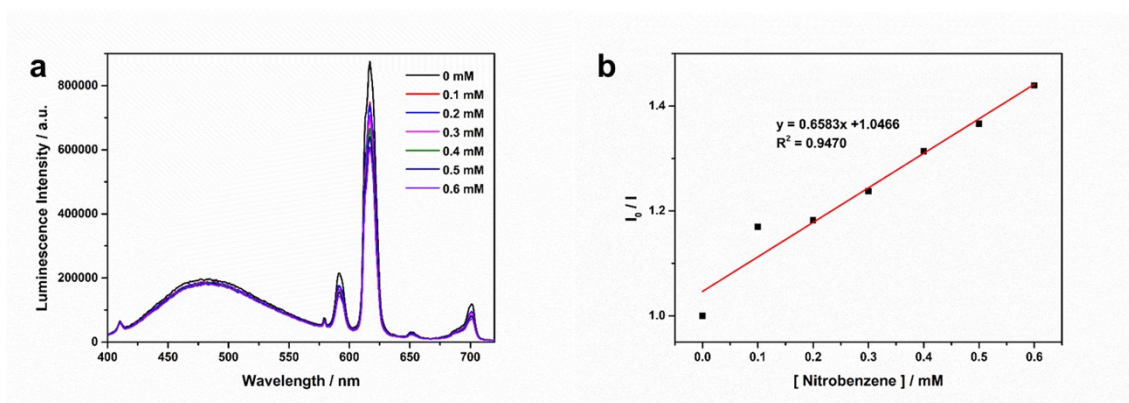
Fig S15. (a) The luminescence spectra of the Eu-MOF recorded with different concentrations of nitrobenzene (0-0.5 mM) in DMAC. (b) SV plot of I_0/I vs increasing concentrations of nitrobenzene.
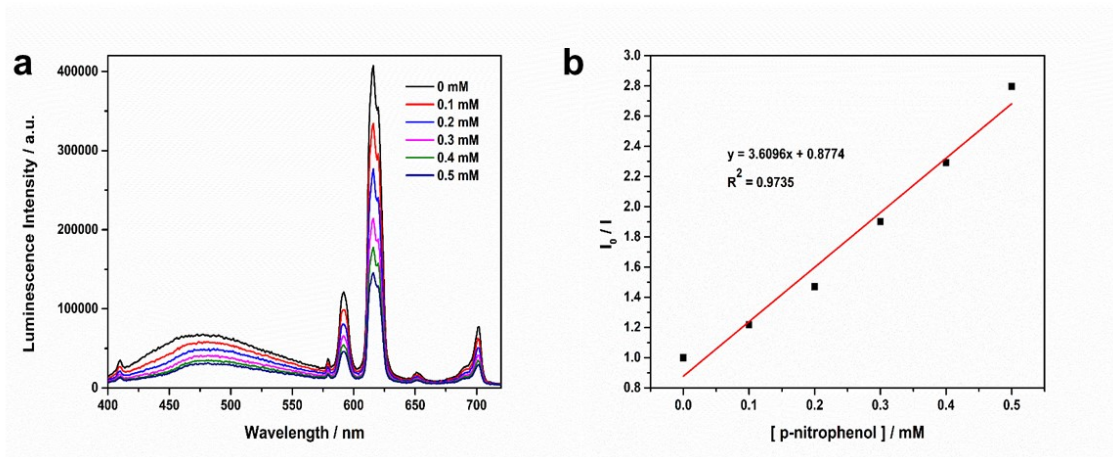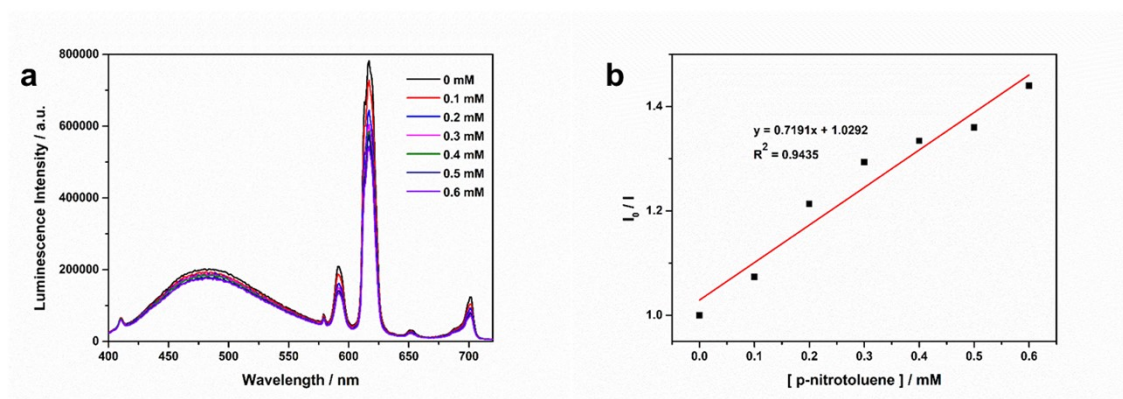

Fig S16. (a) The luminescence spectra of the Eu-MOF recorded with different concentrations of p-nitrotoluene (0-0.5 mM) in DMAC. (b) SV plot of I_0/I vs increasing concentrations of p-nitrotoluene.
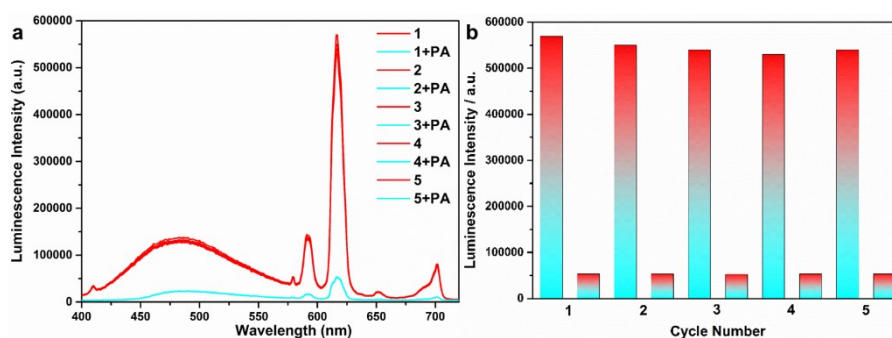
**Fig S17.** Reproducibility of the quenching ability of the Eu-MOF in DMAC and in the presence of PA (0.1 mM). (a) The luminescence spectra of the Eu-MOF in DMAC before and after adding PA; (b) Luminescence intensity at 617 nm before and after adding PA.
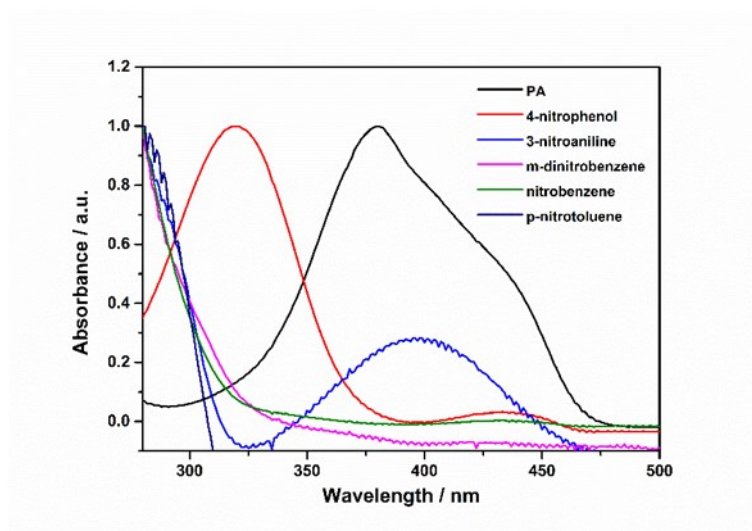
Fig S18. The UV-Vis absorption spectra of nitro explosives in DMAC.
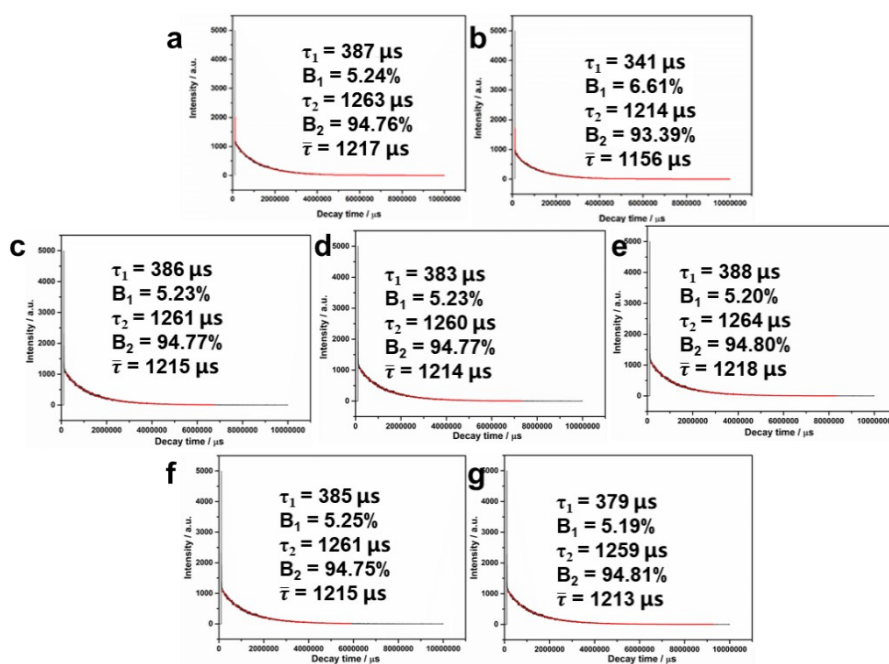
Fig S19. (a)The luminescence decay profiles of the Eu-MOF. (b-g) The luminescence decay profiles of the Eu-MOF mixed with 0.1 mM nitro explosives (PA, p-nitrophenol, 3-nitroaniline, m-dinitrobenzene, nitrobenzene, p-nitrotoluene).
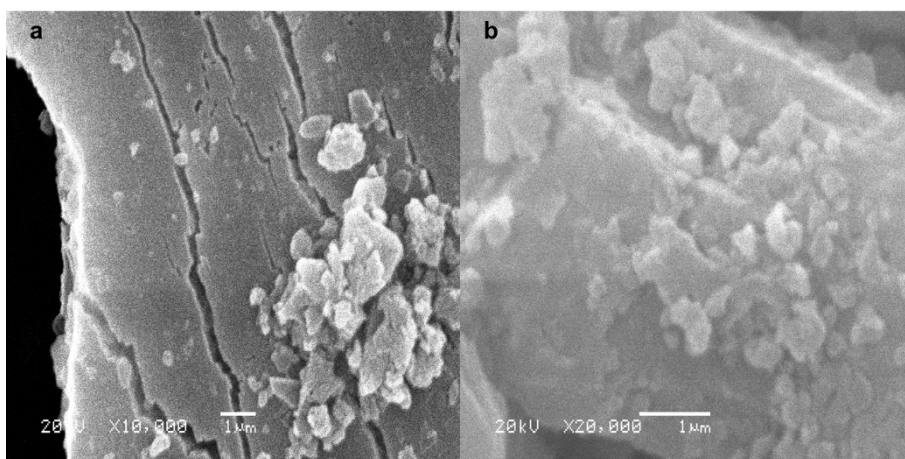
Fig S20. The SEM image of the Eu-MOF before (a) and after (b) detecting PA.

Table S1 Crystal data and structure refinement for the Eu-MOF

Compound	Eu-MOF
Empirical formula	$C_{91}H_{84.5}Eu_2N_9O_{25}$
Formula weight	2008.09
Temperature/K	149.99(10)
Crystal system	monoclinic
Space group	$P2_1/c$
a/Å	17.6657(4)
b/Å	42.3715(9)
c/Å	11.9739(3)
α/°	90
β/°	96.227(2)
γ/°	90
Volume/Å^3	8909.8(4)
Z	4
ρ_{calc}g/cm^3	1.497
μ/mm^{-1}	1.476
F(000)	4078.0

Crystal size/mm^3	0.11 × 0.08 × 0.06
Radiation	Mo Kα (λ = 0.71073)
2Θ range for data collection/°	3.554 to 62.002
Index ranges	-23 ≤ h ≤ 20, -58 ≤ k ≤ 50, -16 ≤ l ≤ 13
Reflections collected	70046
Independent reflections	22526 [R_{int} = 0.0440, R_{sigma} = 0.0515]
Data/restraints/parameters	22526/12/1177
Goodness-of-fit on F^2	1.047
Final R indexes [I>=2σ (I)]	R_1 = 0.0428, wR_2 = 0.0938
Final R indexes [all data]	R_1 = 0.0624, wR_2 = 0.1014

[a]$R1 = \Sigma(|F_o| - |F_c|) / \Sigma|F_o|$; $wR2 = [\Sigma w(|F_o|-|F_c|^2) / \Sigma wFo^2]^{1/2}$

Table S2 The bond length for the Eu-MOF

Atom	Atom	Length/Å
Eu(01)	O(11)	2.330(2)
Eu(01)	O(12)	2.342(2)
Eu(01)	O(13)	2.337(3)
Eu(01)	O(18)^2	2.385(2)
Eu(01)	O(19)^3	2.375(2)
Eu(01)	O(20)^2	2.386(3)
Eu(01)	O(21)^3	2.367(3)
Eu(02)	O(1)^5	2.425(2)
Eu(02)	O(2)^5	2.520(2)
Eu(02)	O(5)	2.647(2)
Eu(02)	O(5)^4	2.525(2)
Eu(02)	O(6)	2.409(2)
Eu(02)	O(7)	2.480(2)
Eu(02)	O(8)	2.403(3)

Eu(02)	O(9)	2.354(2)
Eu(02)	O(10)	2.411(2)

[1]2-X,1-Y,1-Z; [2]+X,+Y,-1+Z; [3]2-X,1-Y,2-Z; [4]1-X,1-Y,1-Z; [5]1-X,1-Y,-Z

Table S3. Calculated excited states and HOMO-LUMO energy levels of the free ligand

Basic set	6-31G(d)					
Excited	Triplet (ev)					Singlet (ev)
state	T_1	T_2	T_3	T_4	T_5	2.3172
Ligand	1.4771	3.1821	3.2108	3.4753	3.6120	535.07 nm
	839.39 nm	389.63 nm	386.15 nm	356.75 nm	343.26 nm	18689 cm^{-1}
	11913 cm^{-1}	25665 cm^{-1}	25897 cm^{-1}	28031 cm^{-1}	29132 cm^{-1}	

Table S4. Comparing the performance of the luminescent MOF thermometers in terms of temperature range, maximum relative sensitivity (S_r) and corresponding temperature (T_m).

Luminescent MOF	Temperature range (K)	S_r (% K^{-1})	T_m (K)	Ref.
$Eu_{0.37}Tb_{0.63}$-BTC-a	313-473	0.68	313	1[1]
$Eu-H_2FDC$	20-320	2.7	170	2[2]
ZJU-88⊃perylene	293-353	1.28	293	3[3]
$Nd_{0.577}Yb_{0.423}BDC-F_4$	293-313	1.20	313	4[4]
$Eu_{0.19}Tb_{0.81}PDDI$	313-473	0.37	473	5[5]
$Eu_{0.05}Tb_{0.95}BDC-OH$	313-513	1.55	440	6[6]
$Tb_{0.99}Eu_{0.01}(BDC)_{1.5}-(H_2O)_2$	290-320	0.31	318	7[7]
EuTPTC-2OMe	313-473	7.78	313	8[8]
$Eu_{0.05}Tb_{0.95}TPTC-2Me$		1.76	353	
$Tb_{0.80}Eu_{0.20}BPDA$	298-318	1.19	313	9[9]
TbTPTC	313-473	1.05	366	10[10]
$Gd_{0.985}Eu_{0.015}TPTC$		0.2	473	
$Gd_{0.9995}Eu_{0.0005}TPTC$		1.5	473	
The Eu-MOF	**120-400**	**2.73**	**400**	**This work**

Table S5. Comparing the performance of the luminescent MOF detecting PA in terms of K_{SV}.

Luminescent MOF	K_{SV} (M^{-1})	Ref.
Eu_4L_3	2001	11[11]
TippMn	118000	12[12]
Eu_2L_3	2912	13[13]
LnCPs 2	26000	14[14]
TbL	4995	15[15]
Pb-MOF	43300	16[16]
Zn-MOF	69500	17[17]
Dy-MOF	85500	18[18]
The Eu-MOF	**53339**	**This work**

Table S6. S-V equations and quenching effect constant (K_{sv}) of various nitro explosives for the Eu-MOF

nitro explosives	S-V equation	K_{SV} (M^{-1})
picric acid	y = 53.3386x + 0.9377	53339
p-nitrophenol	y = 3.6096x + 0.8774	3610
3-nirtoaniline	y = 2.1678x + 0.9761	2168
m-dinitrobenzene	y = 0.8406x + 0.9854	841
nitrobenzene	y = 0.6583x + 1.0466	658
p-nitrotoluene	y = 0.7191x + 1.0292	719

References

1   H. Wang, D. Zhao, Y. Cui, Y. Yang and G. Qian, A Eu/Tb-mixed MOF for luminescent high-temperature sensing, *Journal of Solid State Chemistry*, 2017, **246**, 341–345.

2   L. Li, Y. Zhu, X. Zhou, C. D. S. Brites, D. Ananias, Z. Lin, F. A. A. Paz, J. Rocha, W. Huang and L. D. Carlos, Visible-Light Excited Luminescent Thermometer Based on Single Lanthanide Organic Frameworks, *Adv. Funct. Mater.*, 2016, **26**, 8677–8684.

3   Y. Cui, R. Song, J. Yu, M. Liu, Z. Wang, C. Wu, Y. Yang, Z. Wang, B. Chen and G. Qian, Dual-emitting MOF⊃dye composite for ratiometric temperature sensing, *Advanced materials (Deerfield Beach, Fla.)*, 2015, **27**, 1420–1425.

4   X. Lian, D. Zhao, Y. Cui, Y. Yang and G. Qian, A near infrared luminescent metal-organic framework for temperature sensing in the physiological range, *Chemical communications (Cambridge, England)*, 2015, **51**, 17676–17679.

5   D. Zhao, H. Wang and G. Qian, Synthesis, structure and temperature sensing of a lanthanide-organic framework constructed from a pyridine-containing tetracarboxylic acid ligand, *CrystEngComm*, 2018, **20**, 7395–7400.

6   T. Xia, Z. Shao, X. Yan, M. Liu, L. Yu, Y. Wan, D. Chang, J. Zhang and D. Zhao, Tailoring the triplet level of isomorphic Eu/Tb mixed MOFs for sensitive temperature sensing, *Chemical communications (Cambridge, England)*, 2021, **57**, 3143–3146.

7   A. Cadiau, C. D. S. Brites, P. M. F. J. Costa, R. A. S. Ferreira, J. Rocha and L. D. Carlos, Ratiometric nanothermometer based on an emissive Ln3+-organic framework, *ACS nano*, 2013, **7**, 7213–7218.

8   J. Liu, X. Han, Y. Lu, S. Wang, D. Zhao and C. Li, Isostructural Single- And Dual-Lanthanide Metal-Organic Frameworks Based On Substituent-Group-Modifying Tetracarboxylate Ligands for Ratiometric Temperature Sensing, *Inorganic chemistry*, 2021, **60**, 4133–4143.

9   D. Zhao, X. Rao, J. Yu, Y. Cui, Y. Yang and G. Qian, Design and Synthesis of an MOF Thermometer with High Sensitivity in the Physiological Temperature Range, *Inorganic chemistry*, 2015, **54**, 11193–11199.

10   S. Wang, J. Jiang, Y. Lu, J. Liu, X. Han, D. Zhao and C. Li, Ratiometric fluorescence temperature sensing based on single- and dual-lanthanide metal-organic frameworks, *Journal of Luminescence*, 2020, **226**, 117418.

11   W. Liu, X. Huang, C. Xu, C. Chen, L. Yang, W. Dou, W. Chen, H. Yang and W. Liu, A Multi-responsive Regenerable Europium-Organic Framework Luminescent Sensor for Fe3+ CrVI Anions, and Picric Acid, *Chemistry (Weinheim an der Bergstrasse, Germany)*, 2016, **22**, 18769–18776.

12   Y. Zou, K. Huang, X. Zhang, D. Qin and B. Zhao, Tetraphenylpyrazine-Based Manganese

Metal-Organic Framework as a Multifunctional Sensor for Cu2+, Cr3+, MnO4-, and 2,4,6-Trinitrophenol and the Construction of a Molecular Logical Gate, *Inorganic chemistry*, 2021, **60**, 11222–11230.

13 W. Liu, C. Chen, Z. Wu, Y. Pan, C. Ye, Z. Mu, X. Luo, W. Chen and W. Liu, Construction of Multifunctional Luminescent Lanthanide MOFs by Hydrogen Bond Functionalization for Picric Acid Detection and Fluorescent Dyes Encapsulation, *ACS Sustainable Chem. Eng.*, 2020, **8**, 13497–13506.

14 Y. Liu, Q. Sun, H. Zhou, H. Gao, D. Li and Y. Li, One-dimensional Europium-coordination polymer as luminescent sensor for highly selective and sensitive detection of 2,4,6-trinitrophenol, *Spectrochimica acta. Part A, Molecular and biomolecular spectroscopy*, 2022, **264**, 120303.

15 W. Liu, X. Huang, C. Chen, C. Xu, J. Ma, L. Yang, W. Wang, W. Dou and W. Liu, Function-Oriented: The Construction of Lanthanide MOF Luminescent Sensors Containing Dual-Function Urea Hydrogen-Bond Sites for Efficient Detection of Picric Acid, *Chemistry (Weinheim an der Bergstrasse, Germany)*, 2019, **25**, 1090–1097.

16 S. Yu, K. Y. Zhang, J. X. Li, Y. Xiao, L. X. Sun, F. Y. Bai and Y. H. Xing, Three Pbx(COO)y Cluster Frameworks Based on a Flexible Triazinetricarboxylic Acid Ligand: Syntheses, Structures, and Fluorescent Sensing Application for Nitrophenols, *Inorganic chemistry*, 2021, **60**, 7887–7899.

17 Y.-J. Hu, Y.-M. Li, K. Zheng, W.-H. Zhang, Y.-L. Liu and H. Yang, Construction of a Zn(II)-containing MOF for highly selective detection of picric acid and inhibition of human glioma cell growth, *Journal of Molecular Structure*, 2020, **1202**, 127359.

18 S.-J. Fan, R. Sun, Y.-B. Yan, H.-B. Sun, S.-N. Pang and S.-D. Xu, A Dy(iii)–organic framework as a fluorescent probe for highly selective detection of picric acid and treatment activity on human lung cancer cells, *Open Chemistry*, 2020, **18**, 1105–1116.